Biomass Conversion and Biorefinery (2023) 13:2321–2335
https://doi.org/10.1007/s13399-021-01400-5

ORIGINAL ARTICLE

# Fabrication, characterization, and adsorption applications of low-cost hybride activated carbons from peanut shell-vinasse mixtures by one-step pyrolysis

Esra Arslanoğlu[1] · Muhammet Ş. A. Eren[2] · Hasan Arslanoğlu[3] · Harun Çiftçi[4]

Received: 8 January 2021 / Revised: 19 February 2021 / Accepted: 22 February 2021 / Published online: 27 February 2021


## Abstract

The present work aims to develop an innovative, alternative, fast, and cost-effective one-step pyrolysis method for activated carbon production using peanut shell and vinasse mixture. This facile procedure is based on single-step carbonization treatment at a temperature range of 400–800 °C. Different carbonization time (15–360 min), impregnation ratio (1–3 g/g), impregnation time (3–24 h), and nitrogen flow rate (300 and 600 ml/min) were examined. The chemical and physical properties of the activated carbon examined by SEM-EDX, FT-IR analysis, particle size distribution, iodine number, $pH_{zpc}$, BET surface area, and surface functional group analysis by Boehm's titration. The results illustrate that the values of BET surface area, total pore volume, average pore diameter, iodine number, $pH_{zpc}$, and carbon content of activated carbon were found as 1290.5 $m^2/g$, 0.5667 $cm^3/g$, 21.2 Å, 1258.4 mg/g, 5.7, and 86.89%, respectively.

**Keywords** Peanut shell · Vinasse · One-step pyrolysis · Activated carbon · Precursor · Adsorption

## 1 Introduction

Activated carbon is used in many industrial applications such as removal of inorganic and organic impurities from wastewater treatment, gas/air purification, and chemical and pharmaceutical industry, and also used for recovery of precious metals (gold, silver, platinum) in hydrometallurgy industries. Due to its well-known widespread use as an adsorbent in many processes and also rapid industrial development, the world's demand for activated carbon is increasing consistently. Despite the beneficial use of activated carbon in many applications, the biggest challenge is the high cost of

**Highlights**
- Peanut-vinasse mixtures are a perfect precursor for activated carbon production.
- A new, fast, and economical novel method was developed to produce a well-developed microporosity activated carbon.
- The activated carbon produced is excellent adsorbents to remove dye, iodine, and heavy metals.
- One-step pyrolysis method proved itself to produce rapid, effective, and low-cost activated carbon.
- One-step pyrolysis seriously increased the surface area of activated carbon.

✉ Hasan Arslanoğlu
hasan.arslanoglu@ahievran.edu.tr

Esra Arslanoğlu
esra.falci@ataturk.edu.tr

Muhammet Ş. A. Eren
muhammeteren@iyte.edu.tr

Harun Çiftçi
harunciftci@yahoo.com

[1] Department of Chemical Engineering, Faculty of Engineering Erzurum, Atatürk University, Erzurum, Turkey

[2] Department of Chemical Engineering, Faculty of Engineering, Izmir Institute of Technology, İzmir, Turkey

[3] Department of Chemical Engineering, Faculty of Engineering and Architecture, Kırşehir Ahi Evran University, Kırşehir, Turkey

[4] Department of Medical Biochemistry, Faculty of Medicine, Kırşehir Ahi Evran University, Kırşehir, Turkey

production and long preparation time. For this reason, studies have focused on low-cost activated carbon production in recent years [1–5]. For this reason, the studies on cheap and readily available agricultural waste-based lignocellulosic have been accelerated to achieve low-cost activated carbon production. In this context, many researchers have focused on preparing activated carbon (AC) using various agricultural wastes such as peanut shells [6], bamboo [7], grape stalk [8], watermelon rind [9], and tea industry waste [10] in the literature. Due to its well-known widespread use as an adsorbent in many processes and also rapid industrial development, the world's demand for activated carbon is increasing consistently.

The development of synthesis methods for activated carbon has great importance and there are two methods used as physical and chemical methods. Among these methods, the chemical activation is quite remarkable, because it is suitable to produce micropores and mesoporous carbon materials having high surface area and high pore diameter and porosity [11, 12]. The superior structural properties of the obtained carbon materials, it allows the usage of these materials as the electrode in supercapacitors [13], adsorbent in adsorption processes [14], and hydrogen storage systems [15]. In the chemical activation process, carbonaceous material is heated in the inert medium after impregnation via chemical reagents such as $ZnCl_2$ [16], $(NH_4)_2HPO_4$ [17], $H_3PO_4$ [18], and NaOH [19] for the preparation of activated carbon. These chemical substances, which affect pyrolytic degradation and inhibit the formation of tar, react with the carbonaceous material to produce micro or mesoporous structures [20]. However, the chemical activation method has some drawbacks such as excessive chemical consumption and purification problems. Therefore, a sustainable and simple method is needed for the production of highly porous carbons to overcome these disadvantages [5, 21].

The purpose of this paper has been conducted to find an alternative solution to these challenges. Following this purpose, a cost-effective, rapid method has been developed and called one-step pyrolysis method to produce well-developed microporous activated carbon. In relation to these problems, we suggest a general procedure for the production of activated carbon. It is based on operating of inorganic impurities as precursor. These elements combined with compounds containing carbon and other components due to serve as chemical activation agents during the carbonization process. Especially known as activation agents such as Na, K, and Ca elements enable the formation of mesopores during heat treatment. On the other hand, since they are dispersed homogeneously in the organic matrix and this situation provides chemical activation to be effectively. By this means, porous carbon production can be achieved without using any chemical reagent in only one step [22–24].

Unlike the carbonization studies using inorganic salts for porous carbonaceous material in the literature, we plan to obtain porous material from co-pyrolysis of peanut shell and vinasse which is an easy, one-step, alternative procedure in without using additional chemicals in this study. In this sense, the effects of impregnation ratio and time, activation time, and temperature were also examined the preparation process of activated carbon. Moreover, its textural and some physicochemical characteristics were investigated in detail.

## 2 Materials and methods

### 2.1 Materials

The peanut shell used in the experiments was obtained from a local plant in Adana, Turkey. It was washed with distilled water to remove contaminants from its surface, dried at 80 °C for 24 h, then crushed, and sieved to the desired particle size (−100+200 mesh). The concentrated vinasse as a precursor was supplied from the alcohol production plant of Eskişehir sugar factory, Turkey, and it was used without any pre-treatment in the experiments.

### 2.2 Preparation of activated carbons

The prepared peanut shell and vinasse samples were mixed with a blender at a mixing speed of 22000 rpm to obtain a homogeneous mixture. Samples were taken into 85 mL porcelain crucible. Samples are stored at 100 °C for 48 h; the carbonization was carried out by passing N2 gas at a flow rate of 300 and 600 ml/min (Protherm PLF 110/15) (Fig. 1). The effect of carbonization temperature was investigated for a period of 400, 600, and 800 °C and 120 min at the best time was chosen taking account of the results of a previous series of experiments. The samples in the crucibles taken from the oven were first ground (200 mesh <0.075 mm) and then washed with 2 M HCl solution for 12 h. The activated carbon was separated from the slurry using a filter paper (blue band filter paper por no: 12) and dried in the oven at 105 °C for 12 h. After this procedure, in addition of the characterization studies, the influences of process conditions on the activated carbon production are investigated such as carbonization time, carbonization temperature, and weight of peanut shell/vinasse.

### 2.3 Characterisation of the raw materials and activated carbons

The vinasse and peanut shell were also characterized using proximate and ultimate analysis (LECO CHNS 932 Elemental Analyzer). Vinasse was filled into spectrophotometer cuvettes of known volume and weight. The density was determined by calculating the weighing difference made after

**Fig. 1** Pyrolysis system

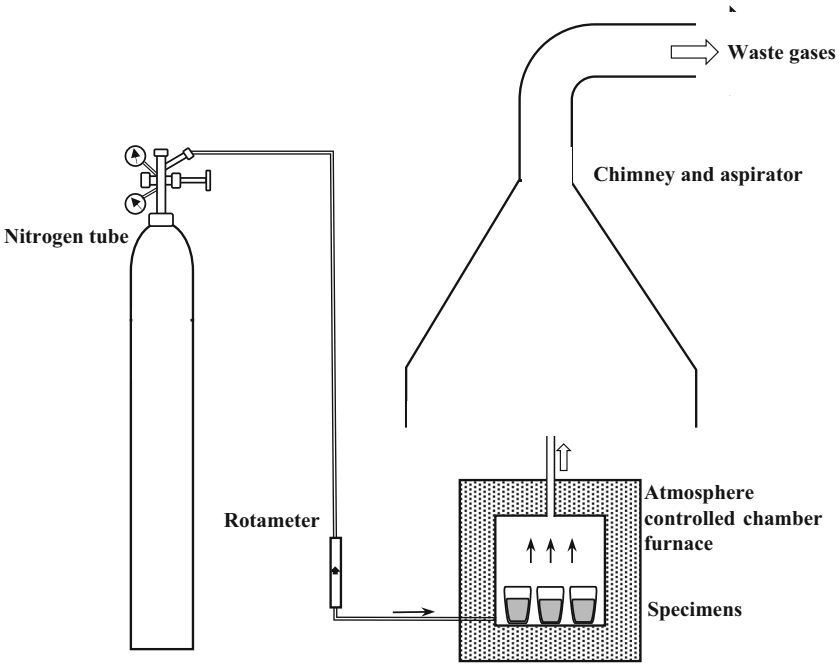


the vibration was well placed. The Fourier transform infrared spectroscopy was used to identify functional groups on the carbon surface. FTIR spectra were recorded 4000-400 $cm^{-1}$ by using Perkin Elmer Spectrum 100. The isoelectric point values of activated carbons were measured with the Malvern Nanosize ZS-3600 zetasizer. Some of the activated carbon solutions were mixed for 2 min in the ultrasonic prop unit. Zeta potentials were measured and the isoelectric point values were read in the device working with laser measurement technique. The particle size distribution of activated carbons was measured by using Malvern Mastersizer 3000. The thermal stability and mass loss of the peanut shell were studied from the thermogravimetric (TG), performed in a simultaneous thermal analysis instrument (PerkinElmer Diamond), using 10 mg aliquots of the sample, subjected to a heating rate of 10 $min^{-1}$ in a nitrogen atmosphere with a flow of 50 mL $min^{-1}$, in a range of 20 to 900 °C. The surface morphology was observed scanning electron microscopy (SEM) technique by using FEI Quanta 250 FEG. The textural properties of the activated carbons were determined by the $N_2$ gas adsorption technique at 77 K using Quanthachrome-Autosorb-1A. The specific surface area of the samples was calculated by the Brunauer-Emmett-Teller (BET) method which assumes that the adsorbent forms more than one layer on the surface. Micropore volume, micropore area, and external surface area were determined with the t-plot method. The pore size distributions were determined via the nonlocal density functional theory (NLDFT) model (Micromeritics ASAP 2020). The activated carbon obtained was examined by $pH_{zpc}$ (Malvern Nanosize ZS-3600 zetasizer) and functional group analysis by Boehm's titration [25]. There are two common characterization methods for used determining the adsorption capacity of activated carbons. The first of these is the iodine number analysis (sodium thiosulfate volumetric method), which is used to measure the adsorption ability of the pores (microporosities) of activated carbon. The amount of iodine (mg) adsorbed by 1 g of activated carbon is called the iodine number and this method was carried out according to ASTM D 4607-94. The other one is the methylene blue analysis, which measures the adsorption capacity of the micro and mesopores of the activated carbons. An appropriate amount of activated carbon was added to the 250 mg/L methylene blue solution. The mixture was stirred for 12 h to ensure that the equilibrium was reached. After 12 h, the mixture was filtered to separate the activated carbon and the methylene blue solution was analyzed at a 660 nm wavelength UV visible spectrophotometer.

## 2.4 Adsorption tests

The equilibrium and adsorption kinetics tests were performed by the batch system. The pH of the 0.25 M copper solution ($CuCl_2.2H_2O$) was not adjusted [26], and therefore, the tests conducted at the buffer solutions (0.07 M sodium acetate–0.03 M acetic acid) pH of the solution (pH 4.8). Initially, equilibrium tests were performed to construct the adsorption isotherms, using 100 mg of the activated carbons and 50 mL of the Cu(II) solutions in concentrations of 50, 100, 150, 200, and 250 mg $L^{-1}$, in 250 mL conical flasks, maintained at 20 °C, 30 °C, 40 °C, 50 °C, and 300 rpm in a shaker incubator (Zcheng D200). The absorbance readings were performed at 1 h intervals until the adsorption equilibrium was established.

The adsorption kinetics was performed using 50 mL of the Cu(II) solutions, in the initial concentration of 100 mg $L^{-1}$ and 50 mg of the adsorbent activated carbons, in 250 mL conical flasks, maintained at 25 °C, 40 °C, 55 °C, and 300 rpm in a shaker incubator (Zcheng D200). Readings were taken at 5, 10, 30, 45, 60, 90, 120, 180, 240, 360, and 720 min. The residual Cu(II) in the aqueous solution was analyzed with a atomic absorbtion spectrophotometer (Perkin Elmer Analyst400). The removal efficiency (%) and the amount of Cu(II) adsorbed (mg/g) were computed by following equations, respectively:

$$\%\text{Cu (II)removal} = (C_o - C_s) \times \frac{100}{C_o} \quad (1)$$

$$q = \frac{(C_o - C_s) \times V}{m} \quad (2)$$

where $C_0$ is the initial Cu(II) concentration (mg $L^{-1}$); $C_s$ is the residual Cu(II) concentration (mg $L^{-1}$) at different contact time intervals. $V$ is the volume of the Cu(II) solution (L), and $m$ is the dosage of the adsorbent (g).

## 3 Results and discussion

### 3.1 Characterization of peanut shell and vinasse

The results of peanut shell and proximate and ultimate analysis are given in Table 1. It is clearly seen that the peanut shell contains 48.94% carbon, moisture 2.3%, and 1.6% ash because of its cellulosic structure. Similarly, the results of elemental analysis of vinasse [27] used as the activation agent in activated carbon production are also given in Table 2. It is seen that it contains significant amounts of potassium, magnesium, sodium, and calcium elements, which serve as precursor during carbonization process. On the other hand, the surface morphology of peanut shell was determined by SEM. As seen from SEM image, it has a rough surface structure with no porosity and no pores (Fig. 2). As a result of determining

**Table 1** Proximate and ultimate analysis of the peanut shell

| Ultimate analysis | wt.% |
|---|---|
| C | 48.94 |
| H | 4.24 |
| N | 0.83 |
| S | 0.15 |
| O | 44.24 |
| Proximate analysis | wt.% |
| Moisture | 2.3 |
| Volatile matter | 69.8 |
| Ash | 1.6 |

**Table 2** Ultimate analysis and some properties of vinasse

| Ultimate analysis | wt.% |
|---|---|
| C | 21.89 |
| H | 7.03 |
| N | 3.14 |
| S | 0.53 |
| O | 21.01 |
| Characteristic | Value |
| Density (g/$cm^3$) | 1.31 |
| pH | 5.3 |
| Ash (950°C) (%) | 9.9 |
| COD (mg-$O_2$/l) | 571000 |
| Brix (Bx) | 63.5 |
| K (mg/kg) | 66500 |
| Na (mg/kg) | 14900 |
| Ca (mg/kg) | 3800 |

all precursor properties, they are suitable for activated carbon production. The ultimate analysis results of biomass used as precursors in the production of activated carbon are given in Table 2. As seen from Table 2, it is generally seen that the precursors' contents are made up of high contents of carbon and oxygen. The fact that the amount of oxygen is almost the same as carbon content can cause large amounts of oxygenated groups in the activated carbon surface. This increases the probability of the surface being acidic in the activated carbon to be obtained [5, 21].

Thermal decomposition properties of the peanut shell were determined by TGA analysis. As shown from TGA curve in Fig. 3, biomass thermal decomposition may be classified into four steps. The first step is that it occurs as a result of the removal of moisture from the biomass at 30–100 °C and

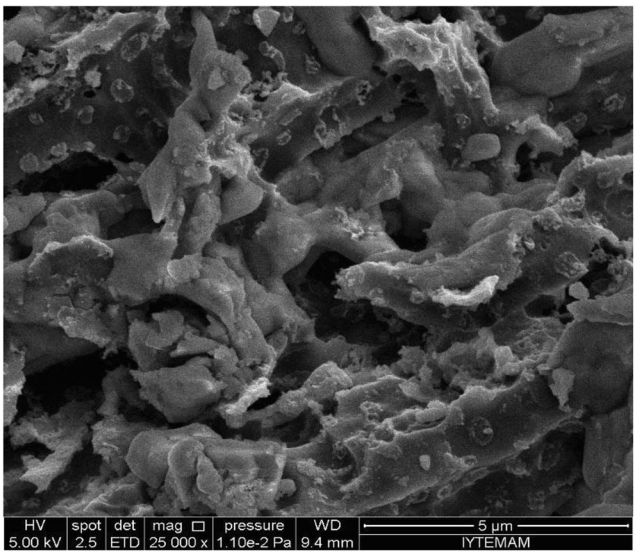


**Fig. 2** SEM image of peanut shell

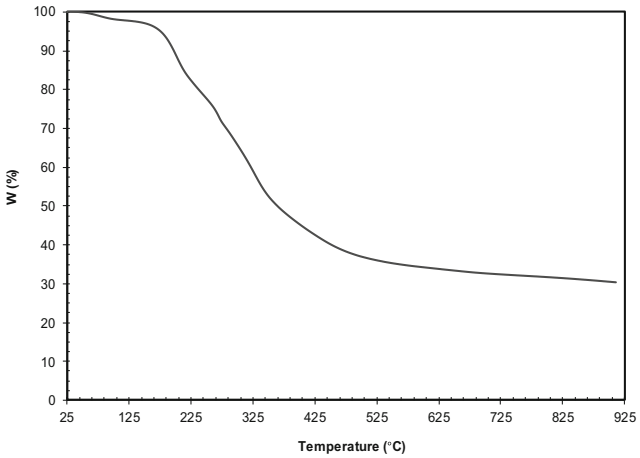


**Fig. 3** TGA diagram of peanut shell

volatiles are removed from the biomass structure at the range of 100–200 °C. The second step includes the decomposing of hemicellulose easily at 220–315 °C. Cellulose decomposition which including the third step happened quickly at 315–400 °C. Lignin is more difficult to decompose than others due to their chemical structure. In the last step, lignin decomposes which occurs very slowly at 200–720 °C. Considering to TGA results, it is seen that thermal degradation is completed around 500 °C. After 500 °C, there is no occurred significant alteration in weight loss of peanut shell. It can be said that temperatures of 500 °C and above are suitable for AC production [28]. Moreover, based on comparable in volatile matter and fixed carbon, the yields of pyrolytic products can be predicted to be significantly different in the three main components. Cellulose contained the highest volatile matter can be expected to reap the highest yields of volatile products, and that of hemicellulose ranked after it. The higher fixed carbon content of lignin can lead to the higher bio-char yields. Different to cellulose, hemicellulose is consisted of various xylose, mannose, glucose, and galactose, and rich of branches, random, amorphous structure appear, which is easy to remove from the main stem and degrade to micromolecular volatiles at low temperatures. At the light of these findings, the all experiments for activated carbon production were performed under the various temperatures (400, 600, and 800°C) and vinasse/peanut shell ratios (1, 1.5, and 2) for 120 min.

## 3.2 Effects of carbonization process parameters

### 3.2.1 Effect of nitrogen flow rate and impregnation time

The experiments were conducted to investigate the influences of impregnation time (3–24 h) and nitrogen flow ratio (300–600 ml/min) under constant conditions; impregnation ratio (vinasse/peanut shell:1), carbonization temperature (600°C), and carbonization time (120 min). The results in Table 3 indicated that surface area was slightly increased due to an increase the impregnation time from 3 to 24 h and varied in the range of 346 to 395 $m^2$/g, respectively. However, there was no noticable increase on surface area as a result of the elevation of nitrogen flow rate [5]. Therefore, the impregnation time was determined to be 24 h for subsequent experiments.

### 3.2.2 Effect of carbonization time

The carbonization time has a critical importance in terms of its high surface area and porosity of the activated carbon.Therefore, a series of experiments were performed at a carbonization time of 15–360 min to assess the influence of time on the some physical properties of the activated carbon when the other process conditions were constant (impregnation ratio, 2; carbonization temperature, 600 °C; and nitrogen flow rate, 300 ml/min.). As shown Table 4, the values of BET surface area and total pore volume continuously increased with the rise of carbonization time up to 120 min. There was no noticable change after this time, whereas the values of BET surface area and total pore volume increased from 160 to 688 $m^2$/g and from 0.1305 to 0.2463 $cm^3$/g with an increase at the carbonization time, respectively. On the other hand, the results demonstrated that the carbonization temperature does not cause any change on the average pore diameter. Percentage carbon values increase in the one-step pyrolysis method. Because of the hold time, oxygen or the other compounds have enough time to remove from the structure. Therefore, their percentage decreases as other compounds get out of the structure. Accordingly, the carbon percentage increases. All in all, activated carbons produced with the one-step pyrolysis method are similar to the conventional pyrolysis method; substantially, one-step pyrolysis method in terms of ash, yield, and porosity has brought advantageous results [5, 29].

### 3.2.3 Effect of carbonization temperature

The peanut shell contains cellulose, hemicellulose, and lignin with decomposition at a temperature range of 230–310, 180–240, and 150–750°C, respectively [30–32]. Therefore, the carbonization experiments were carried out at a temperature ranges of 400–800°C. According to Table 5 and Table 6, the results are illustrated that the BET surface area and the total pore volume generally increase depending on the rise of the carbonization temperature, while the average pore diameter is decreased. In addition, as the carbonization temperature increased from 400 to 800°C, the sorption capacities of methylene blue and iodine number also increased for all impregnation ratio. The highest surface area (1290.5 $m^2$/g) and total pore volume (0.5667 $cm^3$/g) values reached at a temperature of 800°C and impregnation ratio of 3. This state is attributed to the enhancement of porous structure, new pore formation, and surface area because of removal of volatile substances as a result of the increasing carbonization temperature [8].

**Table 3** Determination of nitrogen gas flow rate and impregnation time

| Nitrogen gas flow rate | V/PS ratio (w/w) | Holding time (100°C) (hours) | Pyrolysis time (min) | Pyrolysis temprature (°C) | BET surface area ($m^2$/g) |
|---|---|---|---|---|---|
| 300 ml/min | 1 | 3 | | | 380 |
| | | 6 | | | 367 |
| | | 12 | 120 | 600 | 346 |
| | | 18 | | | 395 |
| | | 24 | | | 371 |
| 600 ml/min | 1 | 3 | | | 395 |
| | | 6 | | | 360 |
| | | 12 | 120 | 600 | 375 |
| | | 18 | | | 389 |
| | | 24 | | | 391 |

### 3.2.4 Effect of impregnation ratio of vinasse/peanut shell

The results of experiments carried out to study the influence of impregnation ratio of vinasse/peanut shell on the activated carbon features are presented in the table. Based on these results, it appears to play an extremely important role on the surface area and porosity of the activated carbon. A raise in the BET surface area of activated carbon from 15.5 to 1290.5 $m^2$/g throughout carbonization process was due to an increase in the impregnation ratio from 1 to 3. This may be explained by the development of microporosity of activated carbon due to the inorganic impurities (Na, Ca, Mg, and K) in vinasse structure serving as the precursor. On the other hand, according to the elemental analysis results in Table 5 and Table 6, it is clearly that the carbon content increases due to the increase of the impregnation ratio. On the contrary of this situation, a rise of the impregnation ratio caused the amounts of O and H decreased. This situation can be attributed to the porosity of the structure, as particles other than carbon are removed from the structure by converting the particles into volatile substances during carbonization. [5, 14, 24, 33].

**Table 4** BET surface areas of the activated carbons obtained under the different activation conditions

| V/P ratio (w/w) | Pyrolysis temperature (°C) | Pyrolysis time (min) | BET surface area ($m^2$/g) | Total pore volume ($cm^3$/g) | Average pore diameter (Å) |
|---|---|---|---|---|---|
| 2 | 600 | 15 | 160 | 0.1305 | 21.1 |
| | | 30 | 279 | 0.1402 | 21.4 |
| | | 45 | 383 | 0.1456 | 21.3 |
| | | 60 | 440 | 0.1534 | 20.8 |
| | | 90 | 530 | 0.1645 | 21.9 |
| | | 120 | 688 | 0.2463 | 22.7 |
| | | 240 | 698 | 0.2455 | 21.6 |
| | | 360 | 684 | 0.2463 | 22.2 |

### 3.2.5 Characterization of activated carbon

FTIR spectra of peanut shell, vinasse, and produced activated carbons are shown in Fig. 4. As can be seen the Fig. 4, peanut shell has O–H stretching vibrations in the range of 3600–3200 $cm^{-1}$ which indicates that the hydroxyl functional groups and absorbed water content [5, 14]. The band at 2920 $cm^{-1}$ indicates the presence of C–H stretching vibrations related to methyl and methylene groups from lignin [34, 35]. The band at 1805 $cm^{-1}$ corresponds to C=O stretching vibrations of carbonyl groups including esters, aldehydes, and ketone in hemicellulose and lignin [35, 36]. The band at 1640–1430 $cm^{-1}$ indicates C=C stretching vibrations in the aromatic ring [37]. The band at 1200–1040 $cm^{-1}$ can be attributed to the C–O vibrations in phenols, ethers, and alcohols [38]. FTIR analysis was performed to determine functional groups of vinasse before the carbonization process. Similar functional groups are observed with the peanut shell spectra. The wide bands 3600–3200 $cm^{-1}$ indicate the absorbed water content. Moreover, the bands at 1640–1430 $cm^{-1}$ are related to C=C ring stretching and strong peaks around 1450–1375 $cm^{-1}$ indicate C–H groups. The FTIR spectra of the activated carbons have fewer bands compared with the FTIR spectra of the peanut shell and vinasse because most of the functional groups are decomposed during carbonization. The -OH band, which is seen around 3600–3200 $cm^{-1}$, originates from the moisture in the structure of the peanut shell, disappeared during the carbonization. The weak bands around the 1560 $cm^{-1}$ indicate C=C vibrations in the benzene ring. The vibration band at 1200–1030 $cm^{-1}$ can be assigned to the C-O vibrations of carboxylate and ether. All of the produced activated carbons with the one-step pyrolysis method have almost the same spectra compared with the conventional pyrolysis method. These findings explain that the one-step pyrolysis method is feasible for activated carbon production [21].

FT-IR and Boehm titration analyses were performed to characterize the functional groups on the activated carbon surface. As a result of Boehm titration, the amounts of carboxylic, phenolic, and lactone, and basic groups on the obtained activated carbon surface were found to be 0.72, 0.33, 0.30, and 0.98 meq/g, respectively. On the other side, in terms of surface functional groups, the amount of total acidic groups is 3.2 times higher than the basic groups (Table 6) [5].

Activated carbons are amphoteric because their surface includes various acidic and basic functional groups that come from raw material. The isoelectric point gives information about external surface charges of the activated carbon; in other words, this is the pH at which the zeta potential is zero. As can be seen from Fig. 5, activated carbon produced with the one-step pyrolysis method has a low isoelectric point

**Table 5** Some physico-chemical characteristics BET surface areas of the activated carbons obtained under the different activation conditions

| V/PS ratio | Pyrolysis temprature (°C) | BET surface area ($m^2$/g) | Total pore volume ($cm^3$/g) | Average pore diameter (Å) | Methylene blue adsorption capacity (mg/g) | Elemental analysis, % | | | | |
|---|---|---|---|---|---|---|---|---|---|---|
| | | | | | | C | H | N | S | O |
| 1 | **400** | 15.5 | 0.0147 | 45.6 | 129.5 | 76.44 | 2.47 | 2.03 | 0.06 | 17.90 |
| | **600** | 241.0 | 0.1093 | 21.8 | 235.3 | 79.21 | 1.40 | 1.92 | 0.17 | 15.81 |
| | **800** | 793.3 | 0.3472 | 20.9 | 531.0 | 80.59 | 0.94 | 1.12 | 0.24 | 14.93 |
| 2 | **400** | 19.0 | 0.0174 | 44.0 | 173.9 | 79.39 | 2.79 | 1.90 | 0.04 | 14.13 |
| | **600** | 598.1 | 0.2463 | 22.7 | 340.0 | 82.55 | 1.43 | 2.22 | 0.36 | 11.40 |
| | **800** | 1196.6 | 0.5458 | 21.9 | 566.0 | 84.97 | 0.83 | 1.09 | 0.28 | 10.35 |
| 3 | **400** | 21.8 | 0.0148 | 32.3 | 203.4 | 82.61 | 2.73 | 2.67 | 0.04 | 9.75 |
| | **600** | 691.4 | 0.2587 | 21.0 | 362.5 | 85.50 | 1.52 | 2.56 | 0.47 | 7.53 |
| | **800** | 1290.5 | 0.5667 | 21.2 | 625.0 | 86.89 | 1.36 | 1.08 | 0.53 | 7.32 |

compared to the conventional pyrolysis method. In other words, having low isoelectric point values refer to more presence of weakly acidic carboxylic functional groups on the surface. As a result of carbonization time, oxygenated groups could not find enough time to remove from the structure so the presence of oxygenated groups remains on the surface. Also, FTIR peaks at 1200–1030 $cm^{-1}$ are related to C–O bonds and this result supports the isoelectric point values. The surface characteristics of the activated carbon used for adsorption processes are determined by $pH_{zpc}$. The pH value of the obtained activated carbon was calculated as 4.51 as shown in Fig. 5. This value confirms the results of Boehm titration, indicating that the acidic groups on the surface are more effective [26, 39].

The iodine number is a preferred method due to determine the surface area, adsorption capacity, and porosity of activated carbons. The iodine number value varies from 500 to 1200 mg/g, which corresponds to surface area values between 900 and 1100 $m^2$/g [40]. On the other hand, considering that the iodine number value of a high-quality activated carbon is greater than 900 mg/g, it is clearly seen that the iodine number of the activated carbon obtained is higher (1258.4 mg/g) (Table 6). When the SEM image of the activated carbon with the highest surface area is examined in Fig. 6, it can be clearly stated that it has a surface with higher porosity than the peanut shell. The difference in size and shape of the pores is due to the fact that the inorganic elements (Na, Mg, Ca, and K) in the vinasse structure serve as activation agents and the volatile substances are removed during the carbonization process. In addition, the structure has become porous and its pores expanded after the elements are completely removed from the structure after washing with acid. SEM images confirm this (Fig. 6). This state indicates that the porosity structure can be enhanced in a single step without using any chemical agent. Based on the elemental analysis (86.89%) (Table 5) and EDS results (85.97%) (Fig. 6) compared in terms of carbon content, it appears that activated carbon has a large amount of carbon content. The particle size distribution of activated carbon having the highest surface area is given in the figure. It was determined that 50% and 10% of the particles have a particle size

**Table 6** Some physico-chemical characteristics of the activated carbons obtained

| V/PS ratio | Pyrolysis temprature (°C) | Ash (%) | Volatile matter (%) | Fixed carbon (%) | $pH_{zpc}$ | Iodine Number (mg/g) | Functional groups (meq/g) | | | | | |
|---|---|---|---|---|---|---|---|---|---|---|---|---|
| | | | | | | | Acidic groups | | | | Basic groups | Total |
| | | | | | | | Carboxylic | Phenolic | Lactonic | Total | | |
| 1 | **400** | 1.10 | 27.48 | 71.41 | | 25.2 | 1.12 | 0.43 | 0.96 | 2.51 | 0.89 | 3.40 |
| | **600** | 1.50 | 21.64 | 76.86 | 3.95 | 287.3 | 1.07 | 0.29 | 0.50 | 1.85 | 0.61 | 2.45 |
| | **800** | 2.18 | 17.17 | 80.65 | | 767.0 | 0.81 | 0.31 | 0.45 | 1.57 | 0.42 | 1.99 |
| 2 | **400** | 1.76 | 17.23 | 81.01 | | 41.1 | 1.47 | 0.52 | 0.73 | 2.72 | 1.06 | 3.77 |
| | **600** | 2.04 | 15.21 | 82.75 | 4.29 | 562.9 | 1.24 | 0.33 | 0.43 | 2.00 | 0.79 | 2.79 |
| | **800** | 2.48 | 12.04 | 85.49 | | 1145.3 | 0.67 | 0.28 | 0.57 | 1.52 | 0.67 | 2.19 |
| 3 | **400** | 2.20 | 12.00 | 85.80 | | 35.4 | 1.41 | 0.43 | 0.80 | 2.64 | 1.19 | 3.83 |
| | **600** | 2.41 | 11.51 | 86.08 | 4.51 | 666.9 | 1.07 | 0.37 | 0.43 | 1.87 | 0.81 | 2.68 |
| | **800** | 2.82 | 10.59 | 86.59 | | 1258.4 | 0.72 | 0.33 | 0.30 | 1.34 | 0.98 | 2.32 |

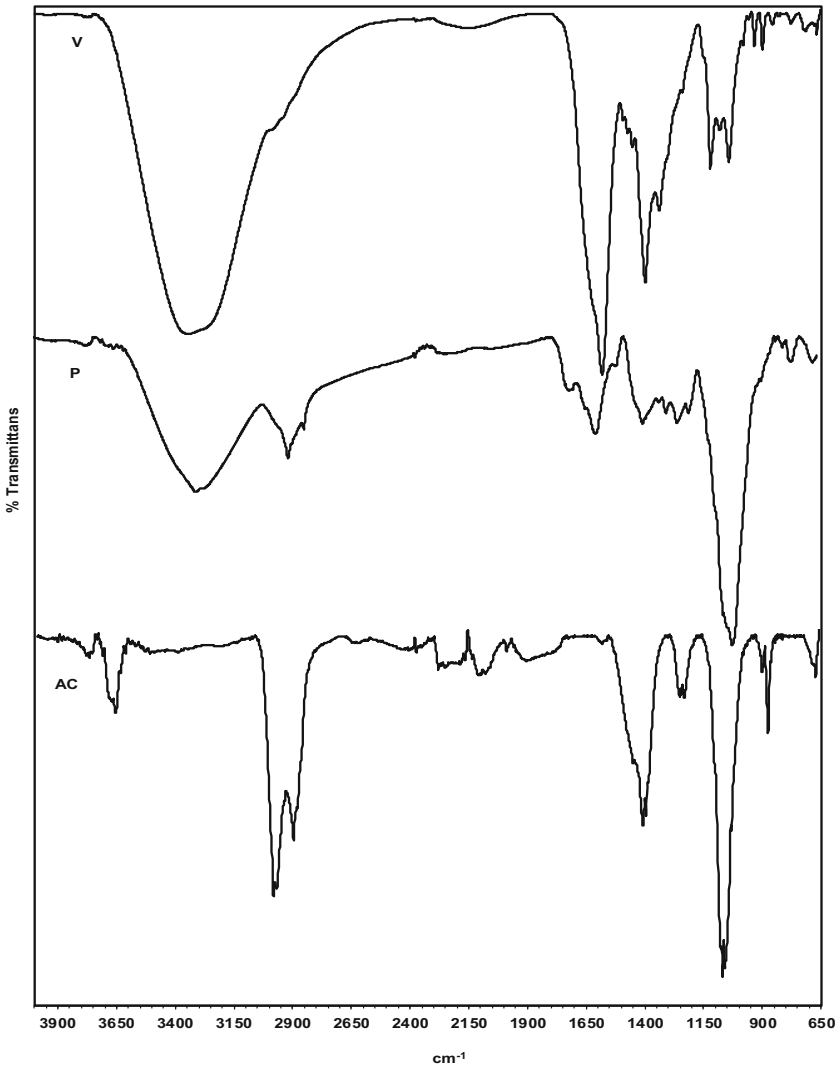


**Fig. 4** FTIR diagram of vinasse, peanut shell, and activated carbon

smaller than 79.119 μm and 35.012 μm, respectively (Fig. 7) [5, 21].

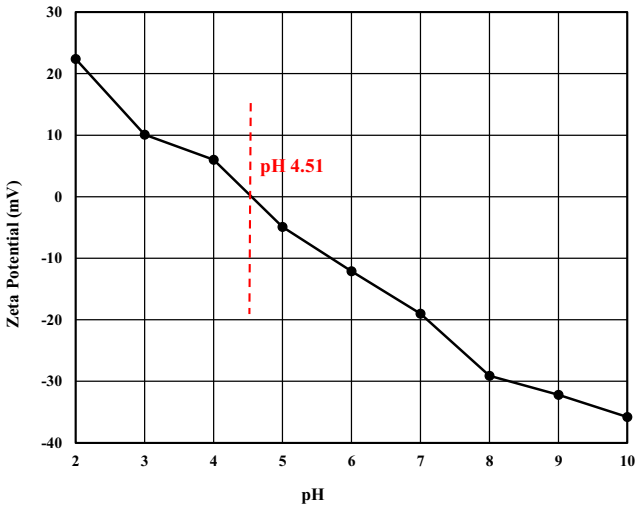


**Fig. 5** pHzpc graph of activated carbon

Adsorption-desorption isotherms under $N_2$ atmosphere at 100 K temperature were plotted to assess the micropore of the obtained activated carbon. According to Fig. 8, the nitrogen isotherm can be defined as type 1 in terms of the physical sorption isotherm classification [41]. Moreover, the total pore volume, pore size, and BET surface area values of the activated carbon under optimum conditions are determined to be 0.5667 $cm^3/g$, 21.2 Å, and 1290.5 $m^2/g$, respectively. These results demonstrated that the activated carbon is microporous.

### 3.3 Activation mechanism

Carbonization and activation carried out in two stages in physical activation are carried out simultaneously in one step and at lower temperatures, and the porous structure is more suitable for various purposes. It is possible to recover the chemicals used. It is known that many chemical substances have been investigated in activated carbon production. ($H_3PO_4$, $ZnCl_2$, KOH (or NaOH), and $K_2CO_3$ (or $Na_2CO_3$)) The selection of

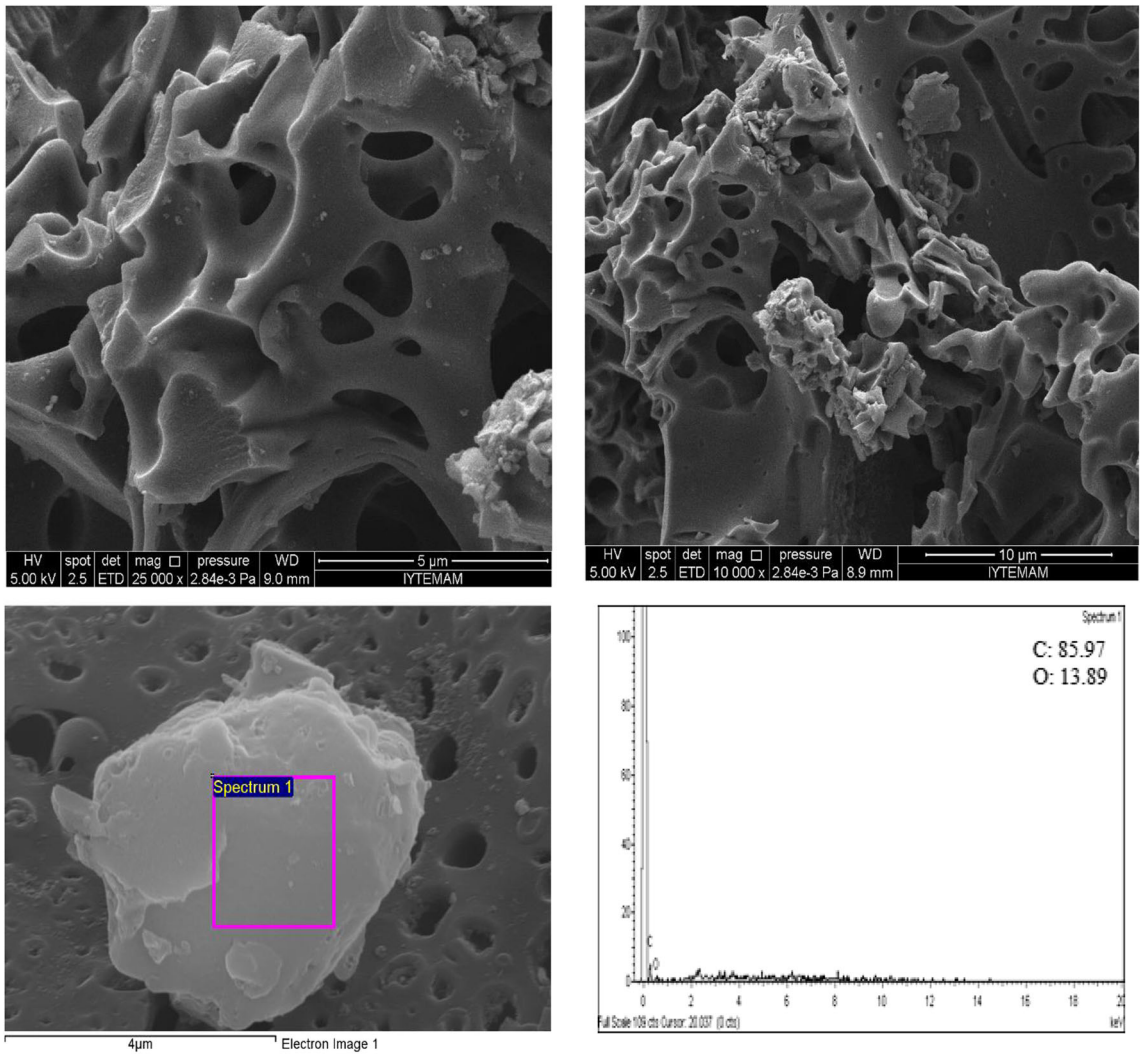


**Fig. 6** SEM image and EDX evaulation of activated carbon

the activation method depends on the starting material (low or high density) and whether powder or granulated activated carbon will be produced [42, 43]. The chemical activation method has advantages such as performing in a single step, requiring a lower temperature and time compared to physical activation, obtaining higher solid product yield, improved

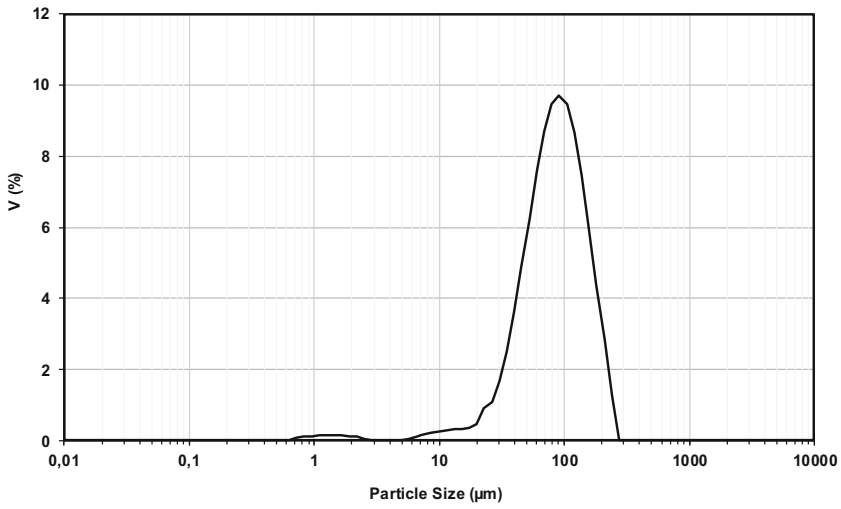


**Fig. 7** Particle size distribution of activated carbon

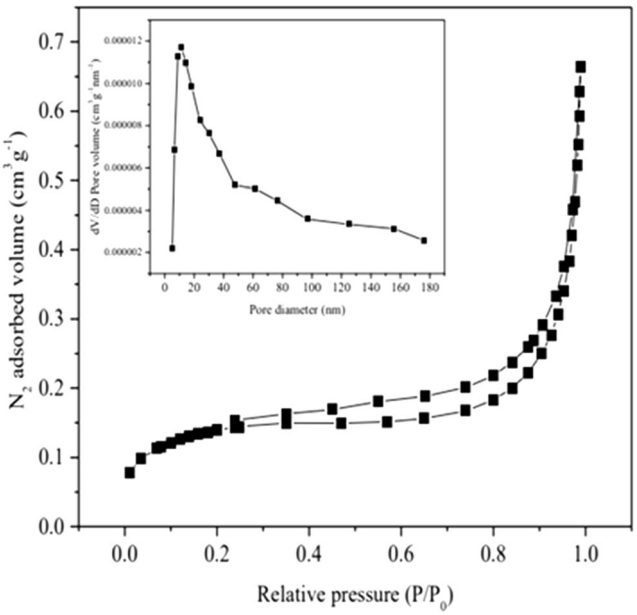


**Fig. 8** Adsorption-desorption isotherms of activated carbon

micropore volume, and larger surface area. Generally, alkali metal salts and especially potassium compounds constitute the important group of chemical activators used in making activated carbon. Due to its close relevance to this study, it is necessary to examine the mechanism of activation with alkali metal compounds.

The surface area and pore size distribution were determined by $N_2$ adsorption-desorption method. Figure 6 presents pore structures of prepared carbons by vinasse activation in this study. Vinasse activation mechanism is a critical step for the development of porosity. Main reactions that occur during the activation are below here [44–46];

During pyrolysis:

$$(C, H, O, N) + Me\ (K\ ve\ Na) \rightarrow Me_2CO_3 + C + CO\uparrow + CO_2\uparrow + H_2O\uparrow + H_2\uparrow + N_2\uparrow \quad (3)$$

The products may also include large molecular tarry substances as a result of degradation and coupling reactions. Other hypothetical events:

$$Me_2CO_3 \rightarrow Me_2O + CO_2\uparrow \quad (4)$$

$$Me_2O + C \rightarrow 2Me + CO\uparrow \quad (5)$$

$$Me + \text{oxygenated compounds} \rightarrow Me_2O + \text{some other compounds} \quad (6)$$

$$Me_2O + H_2O\ (g) \rightarrow 2MeOH \quad (7)$$

$$2Me + 2H_2O\ (g) \rightarrow 2MeOH + H_2\uparrow \quad (8)$$

can be represented as.

To explain the reactions, 700 °C is taken into account. $K_2CO_3$/ $Na_2CO_3$ is starting to form at 400 °C from decomposing KOH/NaOH. With the increasing temperature, it continues to turn into $K_2CO_3$/$Na_2CO_3$, and KOH/NaOH is completely consumed. Thus, carbon structure with the porous network architecture is formed under 700 °C. When the temperature increased to 800 °C, $K_2CO_3$/ $Na_2CO_3$ was almost consumed completely. $K_2CO_3$/ $Na_2CO_3$ and $K_2O$/$Na_2O$ were reduced by carbon to produce metallic K between 800 and 900 °C. Metallic K moves between the carbon lattice of the carbon matrix, thereby expanding the carbon layers and creating new pores. Additionally, the steam and CO2 are produced at high temperatures, which is a physical activation process that contributes to carbon porosity development [5].

Additionally, $K_2CO_3$/ $Na_2CO_3$ has produced these temperature ranges and this means that $K_2CO_3$/$Na_2CO_3$ generates micropores effectively with the one-step pyrolysis method. Metallic K/Na, which occurred between 700 and 800 °C, improved porosity development. These results indicate that not only producing metallic K that generated new pores but also more molecules remove from the structure as increasing temperature are the reasons of obtaining high surface area and micropore volume. At high temperatures like 800 °C, the carbon matrix start to decompose due to the boiling point of metallic K which is 780 °C, that is, some micropores broaden and mesopores are formed [5, 42–45]. Generally, the mesopore surface area is high for some activated carbon samples. Together, these results provide important insights into that high surface area activated carbon (1290.45 $m^2$/g) is produced with the one-step pyrolysis method (Fig. 9).

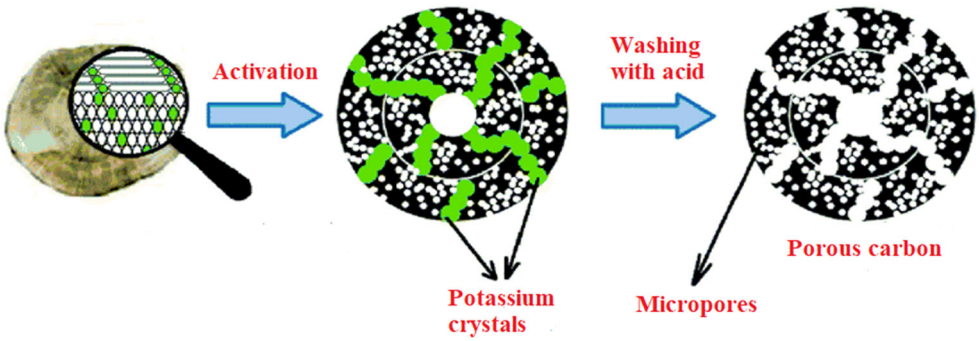


**Fig. 9** Activation mechanism in activated carbon production

**Table 7** Adsorption isotherm models and equations

| Isotherm models | Equations | No |
|---|---|---|
| Langmuir isotherm model | $\frac{C_e}{q_e} = \frac{1}{b \cdot q_m} + \frac{C_e}{q_m}$<br>Plot : $C_e/q_e$ vs. $C_e$ b: Langmuir isotherm constant (L $mg^{-1}$)<br>$q_m$: Maximum adsorption capacity (mg $g^{-1}$) | (9) |
| Freundlich isotherm model | $lnq_e = \frac{1}{m} lnC_e + lnK_f$<br>Plot: $lnq_e$ vs. $lnC_e$ $K_f$: Freundlich isotherm constant related to adsorption capacity (mg $g^{-1}$).(L $mg^{-1}$)$^n$<br>n: Freundlich isotherm constant related to adsorption intensity | (10) |
| DR isotherm model | $lnq_e = ln\ X_m - k_{DR}\varepsilon^2$<br>ln $q_e$ vs. $\varepsilon^2$<br>$X_m$, fluoride adsorption capacity (mg/g)<br>$k$ , D-R isotherm constant<br>$\varepsilon^2$, Polanyi potential | (11) |

## 3.4 Evaluation of Cu(II) removal performance

### 3.4.1 Isotherm studies

The most commonly utilized adsorption isotherm models, viz., Langmuir, Freundlich, and D-R [39, 47, 48] (Table 7) utilized to explore the nature of copper adsorption onto activated carbons with 50–250 mg $L^{-1}$ at different temperatures, viz., 20, 30, 40, and 350 °C are shown in Table 8. The perfect formation of the monolayer after the activation processes can be attributed to the small molecular diameter of the metal molecules that can fully reach the absorbent micropores that make up about 95% of the total surface area of the adsorbent. The monolayer adsorption process of the Langmuir isotherm model illustrates the adsorbent material possesses with homogeneous nature and homogeneous adsorption energy. The linear plot of $C_e$ vs. $C_e/q_e$ is attained from the $Q$ and $b$ of Langmuir coefficients. The heterogeneous nature of the Freundlich isotherm might be affirmed by the direct linear plot of log $q_e$ vs. log $C_e$. The values of $n$ and $k_F$ are obtained from the slope and intercept respectively. The Freundlich isotherm indicates the $n$ values in the range of 1 to 10 and $1/n$ values from 0 to 1 are the favorable conditions for the Cu(II) adsorption process. Additionally, the fitting linear plot of D-R adsorption isotherm was attained by the plot of ln $q_e$ vs. $\varepsilon^2$, and also, the values of parameters such as E with $R^2$, $\chi^2$, and SD are specified in Table 8. In addition, the denote adsorption free energy (E) lying between 8 and 12 kJ $mol^{-1}$ from D-R isotherm indicates that chemisorption involves in the activated carbons towards Cu(II) adsorption process [49]. From the observed results, it clearly indicates Langmuir isotherm was the best fitting model for Cu(II) sorption onto the activated carbons due to higher $R^2$ value and lower $\chi 2$ value and lower SD value which is shown in Table 8. Isotherm equations and their

**Table 8** Calculated isotherm parameters for copper sorption by activated carbons

| Isotherms | Parameters | Temperature (°C) | | | |
|---|---|---|---|---|---|
| | | 20 | 30 | 40 | 50 |
| Langmuir | $Q$ (mg $g^{-1}$ ) | 208.33 | 212.77 | 217.39 | 225.85 |
| | $b$ (L/g) | 0.0316 | 0.0419 | 0.0522 | 0.0599 |
| | $R^2$ | 0.9948 | 0.9916 | 0.9938 | 0.9902 |
| | SD | 1.177 | 1.343 | 1.184 | 1.193 |
| | $\chi 2$ | 0.116 | 0.175 | 0.110 | 0.122 |
| Freundlich | $K_f$ ((mg $g^{-1}$)(l mg)$^{-1/n}$) | 150.642 | 180.018 | 200.564 | 205.236 |
| | 1/n | 0.523 | 0.505 | 0.487 | 0.645 |
| | $R^2$ | 0.9018 | 0.9583 | 0.9362 | 0.9677 |
| | SD | 1.959 | 1.965 | 1.973 | 1.929 |
| | $\chi 2$ | 1.45 | 1.29 | 1.09 | 1.10 |
| Dubinin-Radushkevich (D-R) | Q (mg $g^{-1}$ ) | 247.55 | 257.90 | 272.71 | 280.56 |
| | $E$ | 7.892 | 8.534 | 8.976 | 9.413 |
| | $R^2$ | 0.9856 | 0.9771 | 0.9867 | 0.9967 |
| | SD | 1.610 | 1.626 | 1.618 | 1.645 |
| | $\chi 2$ | 0.326 | 0.331 | 0.337 | 0.339 |

**Table 9** Thermodynamic equations

| Isotherm models | Equations | No |
|---|---|---|
| Enthalpy ($\Delta H°$) | $\ln b = \ln b_0 - \frac{\Delta H^\circ}{RT}$ Plot: lnb vs. 1/T | (12) |
| Free energy ($\Delta G°$) | $\ln\left(\frac{1}{b}\right) = \frac{\Delta G^\circ}{RT}$ | (13) |
| Entropy ($\Delta S°$) | $\Delta G^\circ = \Delta H^\circ - T\Delta S^\circ$ | (14) |

$\Delta G°$, free energy exchange (kJ $mol^{-1}$); $T$ is the absolute temperature ($K$) and $R$ is the universal gas constant (8.314 $Jmol^{-1}$ $K^{-1}$). $b$ can also be expressed in the following equation, including the terms $\Delta H°$ (kJ $mol^{-1}$) and $\Delta S°$ (kJ $mol^{-1}$ $K^{-1}$), as a function of $T$

linear plot details of Langmuir, Freundlich, and D-R were shown in Table 7.

### 3.4.2 Thermodynamic studies

To predict the nature of Cu(II) adsorption on activated carbons was studied using thermodynamic parameters [43]. The thermodynamic parameters such as standard free energy change ($\Delta G°$), standard entropy change ($\Delta S°$), and standard enthalpy change ($\Delta H°$) help to find out the spontaneous and feasible nature of copper adsorption on activated carbons at a given temperature. Thermodynamic parameters, equations, and linear plots of $\Delta G°$, $\Delta S°$, and $\Delta H°$ were given in Table 9. The determined thermodynamic parameter results are shown in Table 10. According to the thermodynamic parameter results obtained, negative values of $\Delta G°$ show that the adsorption of Cu (II) on activated carbons is spontaneous and applicable. The obtained positive values of both $\Delta H°$ and $\Delta S°$ signify Cu(II) adsorption on activated carbons are endothermic nature and irregularity occurred at solid-liquid interfaces of activated carbons with Cu(II) [50, 51].

### 3.4.3 Kinetic studies

The two kinetic models such as reaction-based and diffusion-based kinetic models were utilized for activated carbons towards copper sorption. The reaction-based models such as pseudo-first-order and pseudo-second-order kinetic model [52, 53] were used to find the nature of the reaction rate of Cu(II) adsorption onto the prepared activated carbons was studied at three different temperature conditions (20, 30, 40, and 50 °C). Kinetic models, equations, and their liner plots of first-order and pseudo-second-order were given in Table 11. The direct linear plot of log ($q_e$-$q_t$) vs. $t$ indicates suitability of pseudo first-order model and the appropriateness of the pseudo-second-order kinetic model showed direct linear plot of $t/q_t$ vs. $t$. The applicable values of $k_{ad}$ and $R^2$ of the pseudo-first-order and $q_e$ and $R^2$ values of the pseudo-second-order kinetic model of the prepared activated carbons toward Cu(II) sorption are listed in Table 12 respectively. The $q_e$ value was a little improved with enhance in temperature through Cu(II) sorption. Furthermore, the higher $R^2$ and lower $\chi 2$ values from Table 12 indicate pseudo-second-order kinetic model considers as the best fit model for Cu(II) adsorption process. The diffusion-based kinetic model such as intraparticle diffusion [54, 55] kinetic models was utilized to examine the solute transfer during the solid-solution adsorption method. The appropriateness of the direct linear plot of the intraparticle diffusion kinetic model plot was $q_t$ vs. $t^{0.5}$ respectively. Additionally, the values of $k_{dif}$ and $R^2$ of the particle diffusion and intraparticle diffusion kinetic models toward Cu(II) sorption are demonstrated in Table 12. Therefore, the higher $R^2$ and lower $\chi 2$ values shown from Table 12 indicate intraparticle diffusion kinetic model considers as more applicability for Cu(II) adsorption process onto activated carbons. Kinetic models, equations, and their liner plots of intraparticle diffusion were given in Table 12.

**Table 10** Thermodynamic parameters for copper sorption by activated carbons

| Temperature °C | $\Delta H$ (kj $mol^{-1}$) | $\Delta G$ (kj $mol^{-1}$) | $\Delta S°$ (kJ $mol^{-1}$ $K^{-1}$) |
|---|---|---|---|
| 20 | 12.88 | −8.559 | 0.0722 |
| 30 | | −9.717 | |
| 40 | | −10.783 | |
| 50 | | −11.884 | |

## 4 Conclusions

This paper is the first study to develop a new, alternative one-step pyrolysis method which is called one-step pyrolysis to achieve well-developed microporous activated carbon by offering several advantages: cost-effective, shorter processing time, rapid, and energy savings. Activated carbons with a high total surface area were produced by applying the one-step pyrolysis method from lignocellulosic precursors. The parameters affecting the production process of activated carbon from lignocellulosic wastes were examined in the present study. Thanks to the presence of inorganic elements (Na, Ca, Mg, and K) in vinasse structure, the porous carbon material with a high surface area was produced from peanut shell-vinasse mixture by one-step under optimum process conditions; impregnation ratio, 2; impregnation time, 120 min; carbonization time, 120 min; carbonization temperature, 800°C; and nitrogen flow rate, 300 ml/min. The results illustrate that the values of BET surface area, total pore volume, average pore diameter, iodine number, $pH_{zpc}$, and carbon content of activated carbon were found as 1290.5 $m^2/g$, 0.5667 $cm^3/g$, 21.2 Å, 1258.4 mg/g, 5.7, and 86.89 %, respectively. In addition, it is observed that the active

**Table 11** Adsorption kinetic models and equations

| Kinetic models | Equations | No |
|---|---|---|
| Pseudo-first order model | $\ln(q_e-q_t)=\ln q_e-k_1 t$<br>Plot: ln(qe–qt) vs.t<br>$k_1$: pseudo-first order kinetic rate coefficient ($min^{-1}$) | (15) |
| Pseudo-second order model | $\frac{t}{q}=\frac{1}{k_2 q_e^2}+\frac{t}{q_e}$<br>Plot : $t/q_t$ vs: $t$<br>$k$: pseudo-second order kinetic rate coefficient ($gmg^{-1}\ min^{-1}$) | (16) |
| Intraparticle diffusion model | $q=k_i t^{1/2}+I$<br>Plot : $q_t$ vs: $t^{1/2}$<br>$k_{id}$: ıntraparticle diffusion rate coefficient [$mgg^{-1}\ min^{-1/2}$]<br>$I$: ıntercept related to the thickness of boundary layer<br>$q_e$: adsorption capacity of the adsorbent at the equilibrium ($mg\ g^{-1}$) $q_t$: adsorption capacity of the adsorbent at the time (t) ($mg\ g^{-1}$) | (17) |

carbon surface has a high porosity as well as the presence of acidic functional groups. Consequently, the vinasse and peanut shell are produced in high quantities from sugar factory and agro-industrial, respectively, and cannot be evaluated for any industrial purposes. Therefore, it can be stated that these wastes can be utilized for low-cost activated carbon production. One suggestion is that activated carbon can be produced by one-step pyrolysis method using different biomass species with high cellulose content for future studies. The one-step pyrolysis method is rapid, effective, and low-cost in terms of production method and can also be easily produced commercially. Considering the economical, technological, and ecological balance of the materials produced in general, it is concluded that the activated carbons produced with the one-step pyrolysis method have advantageous characteristics to those produced with conventional pyrolysis.

**Author contribution** Hasan Arslanoğlu: conceptualization, methodology, data curation, ınvestigation, and writing—original draft preparation. Esra Arslanoğlu: visualization, investigation. M.Şakir Eren: methodology, and data curation. Harun Çiftçi: conceptualization, methodology, and writing—review and editing.

## Declarations

**Competing ınterests** The authors declare no competing interests.

**Table 12** Calculated model parameters and regression coefficients for kinetic (pseudo-first-order, pseudo-second-order, and intraparticle diffusion) models for various temperatures

| Kinetic models | Parameters | Temperature | | | |
|---|---|---|---|---|---|
| | | 20°C | 30°C | 40°C | 50°C |
| Pseudo First Order | Equation | $y=-0.0587x+4.042$ | $y=-0.00188x+3.205$ | $y=-0.0299x+3.7038$ | $y=-0.0399x+4.2038$ |
| | $k_1$ ($l\ min^{-1}$) | 0.0587 | 0.0188 | 0.0299 | 0.0399 |
| | $q_{cal}$ ($mg\ g^{-1}$) | 155.42 | 200.12 | 255.36 | 265.99 |
| | $R^2$ | 0.9303 | 0.9255 | 0.9408 | 0.9623 |
| | $X^2$ | 10.8317 | 7.1740 | 6.2970 | 5.2325 |
| Pseudo Second Order | Equation | y=0.0054x+0.2297 | y=0.0068x+0.1905 | y=0.0083x+0.1171 | $y=0.0089x+0.1256$ |
| | $k_2$ ($g\ (mg.min)^{-1}$) | 0.0054 | 0.0068 | 0.0083 | 0.0089 |
| | $q_{cal}$ (mg/g) | 195.15 | 237.86 | 277.14 | 299.23 |
| | $R^2$ | 0.9927 | 0.9934 | 0.9975 | 0.9965 |
| | $X^2$ | 0.0087 | 0.0001 | 0.0059 | 0.0055 |
| Intra Particle Diffusion | Equation | $y=0.2219x+20.55$ | $y=0.2514x+30.78$ | $y=0.4757x+45.72$ | $y=0.4951x+45.72$ |
| | $k_{dif}$ ($mg\ (g\ min^{0.5})^{-1}$) | 0.2219 | 0.2514 | 0.4757 | 0.4951 |
| | $q_{cal}$ (mg/g) | 179.55 | 220.78 | 277.72 | 285.12 |
| | $R^2$ | 0.9814 | 0.9859 | 0.9865 | 0.9760 |
| | $X^2$ | 1.5907 | 1.3447 | 1.1332 | 1.3266 |

## References


1. Zhai Y, Dou Y, Zhao D, Fulvio PF, Mayes RT, Dai S (2011) Carbon materials for chemical capacitive energy storage. Adv Mater 23(42):4828–4850
2. Kaskhedikar NA, Maier J (2009) Lithium storage in carbon nanostructures. Adv Mater 21(25-26):2664–2680
3. Jordá-Beneyto M, Suárez-García F, Lozano-Castelló D, Cazorla-Amorós D, Linares-Solano A (2007) Hydrogen storage on chemically activated carbons and carbon nanomaterials at high pressures. Carbon 45(2):293–303
4. Calvino-Casilda V, López-Peinado AJ, Durán-Valle CJ, Martín-Aranda RM (2010) Last decade of research on activated carbons as catalytic support in chemical processes. Catal Rev 52(3):325–380
5. Arslanoğlu H (2019) Direct and facile synthesis of highly porous low cost carbon from potassium-rich wine stone and their application for high-performance removal. J Hazard Mater 374:238–247
6. Georgin J, Dotto GL, Mazutti MA, Foletto EL (2016) Preparation of activated carbon from peanut shell by conventional pyrolysis and microwave irradiation-pyrolysis to remove organic dyes from aqueous solutions. J Environ Chem Eng 4(1):266–275
7. Wang YX, Ngo HH, Guo WS (2015) Preparation of a specific bamboo based activated carbon and its application for ciprofloxacin removal. Sci Total Environ 533:32–39
8. Ozdemir I, Şahin M, Orhan R, Erdem M (2014) Preparation and characterization of activated carbon from grape stalk by zinc chloride activation. Fuel Process Technol 125:200–206
9. Üner O, Geçgel Ü, Bayrak Y (2015) Preparation and characterization of mesoporous activated carbons from waste watermelon rind by using the chemical activation method with zinc chloride. Arab J Chem 12(8):3621–3627
10. Gundogdu A, Duran C, Senturk HB, Soylak M, Imamoglu M, Onal Y (2013) Physicochemical characteristics of a novel activated carbon produced from tea industry waste. J Anal Appl Pyrolysis 104: 249–259
11. Molina-Sabio M, Rodrıguez-Reinoso F (2004) Role of chemical activation in the development of carbon porosity. Colloid Surf A: Physicochem Eng Asp 241(1-3):15–25
12. Lozano-Castello D, Calo JM, Cazorla-Amoros D, Linares-Solano A (2007) Carbon activation with KOH as explored by temperature programmed techniques, and the effects of hydrogen. Carbon 45(13):2529–2536
13. Wei L, Sevilla M, Fuertes AB, Mokaya R, Yushin G (2011) Hydrothermal carbonization of abundant renewable natural organic chemicals for high-performance supercapacitor electrodes. Adv Energy Mater 1(3):356–361
14. Seyrek EŞ, Yalcin E, Yilmaz M, Kök BV, Arslanoğlu H (2020) Effect of activated carbon obtained from vinasse and marc on the rheological and mechanical characteristics of the bitumen binders and hot mix asphalts. Constr Build Mater 240:117921
15. Sevilla M, Fuertes AB, Mokaya R (2011) High density hydrogen storage in superactivated carbons from hydrothermally carbonized renewable organic materials. Energy Environ Sci 4(4):1400–1410
16. Angin D (2014) Production and characterization of activated carbon from sour cherry stones by zinc chloride. Fuel 115:804–811
17. Gao P, Liu ZH, Xue G, Han B, Zhou MH (2011) Preparation and characterization of activated carbon produced from rice straw by (NH4) 2HPO4 activation. Bioresour Technol 102(3):3645–3648
18. Kumar A, Jena HM (2016) Preparation and characterization of high surface area activated carbon from Fox nut (Euryale ferox) shell by chemical activation with H3PO4. Results Phys 6:651–658
19. Islam MA, Ahmed MJ, Khanday WA, Asif M, Hameed BH (2017) Mesoporous activated carbon prepared from NaOH activation of rattan (Lacosperma secundiflorum) hydrochar for methylene blue removal. Ecotoxicology and environmental safety 138:279–285
20. Arslanoğlu H, Tümen F (2021) Potassium struvite (slow release fertilizer) and activated carbon production: resource recovery from vinasse and grape marc organic waste using thermal processing. Process Saf Environ 147(March):1077–1087
21. Arslanoğlu H, Kaya S, Tümen F (2019) Cr (VI) adsorption on low-cost activated carbon developed from grape marc-vinasse mixture. Particul Sci Technol 38(6):768–781
22. Sevilla M, Fuertes AB (2013) A general and facile synthesis strategy towards highly porous carbons: carbonization of organic salts. J Mater Chem A 1(44):13738–13741
23. Sevilla M, Fuertes AB (2014) Direct synthesis of highly porous interconnected carbon nanosheets and their application as high-performance supercapacitors. ACS nano 8(5):5069–5078
24. Arslanoğlu H, Orhan R, Turan MD (2019) Application of response surface methodology for the optimization of copper removal from aqueous solution by activated carbon prepared using waste polyurethane. Anal Lett 53(9):1343–1365
25. Boehm HP (2002) Surface oxides on carbon and their analysis: a critical assessment. Carbon 40(2):145–149
26. Shi Y, Zhu J, Yuan G, Liu G, Wang Q, Sun W, Zhang H (2020) Activation of persulfate by EDTA-2 K-derived nitrogen-doped porous carbons for organic contaminant removal: radical and non-radical pathways. Chem Eng J 386:124009
27. Arslanoğlu H (2016) Development of a process for producing slow released potassium-struvite fertilizer from vinasse and grape marc. PhD thesis, Firat University, Turkey, Elazığ (In Turkish).
28. Djilani C, Zaghdoudi R, Modarressi A, Rogalski M, Djazi F, Lallam A (2012) Elimination of organic micropollutants by adsorption on activated carbon prepared from agricultural waste. Chem Eng J 189:203–212
29. Wang L, Sun F, Hao F, Qu Z, Gao J, Liu M, Qin Y (2020) A green trace K2CO3 induced catalytic activation strategy for developing coal-converted activated carbon as advanced candidate for CO2 adsorption and supercapacitors. Chem Eng J 383:123205
30. Zeriouh A, Belkbir L (1995) Thermal decomposition of a Moroccan wood under a nitrogen atmosphere. Thermochim acta 258:243–248
31. Nunn TR, Howard JB, Longwell JP, Peters WA (1985) Product compositions and kinetics in the rapid pyrolysis of sweet gum hardwood. Ind Eng Chem Process Des Dev 24(3):836–844
32. Tsamba AJ, Yang W, Blasiak W (2006) Pyrolysis characteristics and global kinetics of coconut and cashew nut shells. Fuel Process Technol 87(6):523–530
33. Li Z, Hanafy H, Zhang L, Sellaoui L, Netto MS, Oliveira ML, Li Q (2020) Adsorption of congo red and methylene blue dyes on an ashitaba waste and a walnut shell-based activated carbon from aqueous solutions: experiments, characterization and physical interpretations. Chem Eng J 388:124263
34. Yang T, Lua AC (2003) Characteristics of activated carbons prepared from pistachio-nut shells by physical activation. J Colloid Interface Sci 267:408–417
35. Park SH, McClain S, Tian ZR, Suib SL, Karwacki C (1997) Surface and bulk measurements of metals deposited on activated carbon. Chem Mater 9:176–183
36. Al-Qodah Z, Shawabkah R (2009) Production and characterization of granular activated carbon from activated sludge. Braz J Chem Eng 26:127–136
37. Attia AA, Rashwan WE, Khedr SA (2006) Capacity of activated carbon in the removal of acid dyes subsequent to its thermal treatment. Dyes Pigm 69:128–136
38. Figueiredo JL, Pereira MFR, Freitas MMA, Orfao JJM (1999) Modification of the surface chemistry of activated carbons. Carbon 37:1379–1389

39. Arslanoglu H (2019) Adsorption of micronutrient metal ion onto struvite to prepare slow release multielement fertilizer: copper (II) doped-struvite. Chemosphere 217:393–401
40. Elliott C, Colby T, Iticks H (1989) Activated carbon obliterans alter aspiration of activated charcoal. Chest 96(3):672–674
41. Sing KS (1985) Reporting physisorption data for gas/solid systems with special reference to the determination of surface area and porosity (Recommendations 1984). Pure Appl Chem *57*(4):603–619
42. Joseph CG, Zain HFM, Dek SF (2006) Treatment of landfill leachate in Kayu Madang, Sabah: textural and physical characterization (part 1). Malays J Anal Sci 10(1):1–6
43. Hui TS, Zaini MAA (2015) Potassium hydroxide activation of activated carbon: a commentary. Carbon Lett 16(4):275–280
44. Guo J, Lua AC (2002) Textural and chemical characterizations of adsorbent prepared from palm shell by potassium hydroxide impregnation at different stages. J Colloid Interface Sci 254(2):227–233
45. Lillo-Ródenas MA, Cazorla-Amorós D, Linares-Solano A (2003) Understanding chemical reactions between carbons and NaOH and KOH: an insight into the chemical activation mechanism. Carbon 41(2):267–275
46. Alcañiz-Monge J, Illán-Gómez MJ (2008) Insight into hydroxides-activated coals: chemical or physical activation? J Colloid Interface Sci 318(1):35–41
47. Arslanoglu H (2017) Removal of Cu (II) from aqueous solutions by using marble waste. Pamukkale Univ J Eng Sci 23(7):877–886
48. Kim DW, Wee JH, Yang CM, Yang KS (2020) Efficient removals of Hg and Cd in aqueous solution through NaOH-modified activated carbon fiber. Chem Eng J 392:123768
49. Yaraş A, Arslanoğlu H (2018) Valorization of paper mill sludge as adsorbent in adsorption process of copper (II) ion from synthetic solution: kinetic, isotherm and thermodynamic studies. Arabian J Sci Eng 43(5):2393–2402
50. Zhang T, Wang W, Zhao Y, Bai H, WenT, Kang S, Komarneni S (2020) Removal of heavy metals and dyes by clay-based adsorbents: From natural clays to 1D and 2D nano-composites. Chem Eng J 127574.
51. Yaraş A, Arslanoğlu H (2019) Utilization of paper mill sludge for removal of cationic textile dyes from aqueous solutions. Sep Sci Technol 54(16):2555–2566
52. Li H, Zheng F, Wang J, Zhou J, Huang X, Chen L, Liu JL (2020) Facile preparation of zeolite-activated carbon composite from coal gangue with enhanced adsorption performance. Chem Eng J 390: 124513
53. Yaraş A, Arslanoğlu H (2018) Efficient removal of basic yellow 51 dye via carbonized paper mill sludge using sulfuric acid. Sigma J Eng Nat Sci 36(3):803–818
54. Arslanoğlu H (2021) Production of low-cost adsorbent with small particle size from calcium carbonate rich residue carbonatation cake and their high performance phosphate adsorption applications. J Mater Res Technol 11(March-April):428–447
55. Eren MŞ, Arslanoğlu H, Çiftçi H (2020) Production of microporous Cu-doped BTC (Cu-BTC) metal-organic framework composite materials, superior adsorbents for the removal of methylene blue (Basic Blue 9). J Environ Chem Eng 8(5):104247